

Lectures at International School of Space Science, L'Aquila, Italy, August-September 2001
To be published in the Frascati Physics Series by S.I.S.-Laboratori Nazionali di Frascati.

PROBING GALAXY FORMATION WITH HIGH ENERGY GAMMA-RAYS

Joel R. Primack

Physics Department, University of California, Santa Cruz, CA 95064 USA

ABSTRACT

I discuss how measurements of the absorption of γ -rays from GeV to TeV energies via pair production on the extragalactic background light (EBL) can probe important issues in galaxy formation. My group uses semi-analytic models (SAMs) of galaxy formation, set within the CDM hierarchical structure formation scenario, to obtain predictions of the EBL from 0.1 to 1000 μm . SAMs incorporate simplified physical treatments of the key processes of galaxy formation — including gravitational collapse and merging of dark matter halos, gas cooling and dissipation, star formation, supernova feedback and metal production — and have been shown to reproduce key observations at low and high redshift. We have improved our modelling of the spectral energy distributions in the mid-to-far-IR arising from emission by dust grains. Assuming a flat Λ CDM cosmology with $\Omega_m = 0.3$ and Hubble parameter $h = 0.65$, we investigate the consequences of variations in input assumptions such as the stellar initial mass function (IMF) and the efficiency of converting cold gas into stars. We also discuss recent attempts to determine the emitted spectrum of high

energy gamma rays from blazars such as Mrk 501 using the synchrotron self-Compton model and the observed X-rays, and note that our favorite SAM EBL plus the observed spectrum of Mrk 501 do *not* imply unphysical upturns in the high energy emitted spectrum — thus undermining recent claims of a crisis with drastic possible consequences such as breaking of Lorentz invariance. We conclude that observational studies of the absorption of γ -rays with energies from ~ 10 GeV to ~ 10 TeV will help to determine the EBL, and also help to explain its origin by constraining some of the most uncertain features of galaxy formation theory, including the IMF, the history of star formation, and the reprocessing of light by dust.¹

1 Introduction

The extragalactic background light (EBL) represents all the light that has been emitted by galaxies over the entire history of the universe. The EBL that we observe today is an admixture of light from different epochs, its spectral energy distribution (SED) distorted by the redshifting of photons as they travel to us from sources at different distances. It is therefore a constraint on both the intrinsic SEDs of the sources and their distribution in redshift. At present, there is more than a factor of two uncertainty in the amplitude of the EBL in the UV, optical, and near-infrared ²⁾. The EBL in the mid-IR is even more uncertain. The far-IR background measured at $\gtrsim 100\mu\text{m}$ ^{3, 4, 5, 6)} represents at least half of the total energy in the EBL, yet the sources that produced it remain uncertain.

High energy γ -ray astronomy promises to help resolve these uncertainties by providing independent constraints on the EBL, in the mid-IR with E_γ in the ~ 10 TeV energy range, and in the $0.1\text{-}3\ \mu\text{m}$ range with $E_\gamma \sim 100$ GeV via the new low-threshold instruments that will soon be available. High energy γ -rays from sources at cosmological distances are absorbed via electron-positron pair production on the diffuse background of photons that comprises the EBL. Thus, γ -ray observations of objects with known redshift and intrinsic spectral shape will constrain the EBL in these crucial wavelength regimes by measuring the optical depth of the Universe to photons of various energies. This in turn will help to constrain some of the most fundamental uncertainties in physical

¹This paper is an updated version of ¹⁾.

models of galaxy formation.

In order to illustrate this, in this paper we use a “forward evolution” approach, which attempts to model the essential features of galaxy formation using simple recipes. These semi-analytic models are set within the modern Cold Dark Matter (CDM) paradigm of hierarchical structure formation, and trace the gravitational collapse and merging of dark matter halos, the cooling and shock heating of gas, star formation, supernovae feedback, metal production, the evolution of stellar populations and the absorption and re-emission of starlight by dust. This machinery has been used extensively to predict optical properties of low-redshift galaxies, with good results (e.g., ^{7, 8}); reviewed and extended in ^{9, 10}, hereafter SP and SPF). A semi-analytic approach was also used by Devriendt and Guiderdoni ¹¹) to make predictions of counts and backgrounds in the mid-to-far-IR, with more detailed modelling of dust extinction and emission, but less detailed modelling of merging and star formation. We have now combined the strengths of these two approaches, by integrating the stellar SEDs and dust modelling of ^{12, 11}) into the galaxy formation SAM code of the Santa Cruz group.

Some parts of the “standard paradigm” of galaxy formation represented by our SAMs are relatively solid. For example, once a cosmological model and power spectrum are specified, it is straightforward to compute the gravitational collapse of dark matter into bound halos using N -body techniques, and analytic formalisms such as those used in our modelling ¹³) have been checked against these results ¹⁴). Within the range of values for the cosmological parameters allowed by existing observational constraints (i.e., $\Omega_{\text{matter}} \simeq 0.3 - 0.5$, $\Omega_{\text{matter}} + \Omega_{\Lambda} \simeq 1$, $H_0 \simeq 60 - 80$ km/s/Mpc; see e.g. ¹⁵) for a summary), these results do not change significantly. Similarly, modelling of gas cooling appears to be fairly robust and agrees well with hydrodynamic simulations ¹⁶). However, other aspects, notably the efficiency of conversion of cold gas into stars, the effect of subsequent feedback due to supernovae winds or ionizing photons, the stellar initial mass function (IMF), and the effects of dust, remain highly uncertain, and some predictions are quite sensitive to their details.

For example, SPF showed that the star formation history of the Universe and the number density of high redshift $z \gtrsim 2$ “Lyman-break” galaxies (LBGs; e.g. ¹⁷) may be quite different depending on whether star formation is primarily regulated by internal properties, such as gas surface density in a quiescent

disk, or triggered by an external event such as an interaction. Because the largest samples of LBGs are primarily identified in the rest UV, model predictions are also quite sensitive to the high-stellar-mass slope of the IMF, and to dust extinction. At the other end of the spectrum is the sub-mm population detected by SCUBA, believed to be predominantly high redshift ($z \gtrsim 2$) luminous and ultraluminous infrared galaxies (LIRGs and ULIRGs) powered by star formation rates of hundreds to thousands of solar masses per year (e.g., 18). Theoretical predictions of the numbers and nature of these objects are highly sensitive to the same issues (the dominant mode of star formation, dust, the IMF), but provide a crucial counter-balance to the optical observations. However, the current mismatch between the sensitivity and spatial resolution of optical and sub-mm instrumentation has made it difficult to establish the connection between the two populations observationally.

The Milky Way, like most nearby galaxies, emits the majority of its light in optical and near-IR wavelengths; only about 30% of the bolometric luminosity locally is released in the far-infrared¹⁹⁾. This was generally believed to be typical of most of the starlight at all redshifts until the discovery of the far-IR part of the EBL by the DIRBE and FIRAS instruments on the COBE satellite, at a level ten times higher than the no-evolution predictions based on the local luminosity function of IRAS galaxies, and representing twice as much energy as the optical background obtained from counts of resolved galaxies²⁰⁾. This result suggests that either the dust extinction properties of “normal” galaxies change dramatically with redshift, or a population of heavily extinguished galaxies (perhaps analogous to local LIRGs and ULIRGs) is much more common at high redshift than locally, or both. Some of these galaxies may have already been observed, at 15 μm by ISO²¹⁾, and at 850 μm by SCUBA²²⁾.

Guideroni et al.^{23, 11)} showed that their simplified semi-analytic model could reproduce the multi-wavelength data only if they introduced a population of heavily extinguished galaxies with high star formation rates, and with strong evolution of number density with redshift. This population was introduced ad-hoc by^{23, 11)}, but as discussed by these authors, by²⁴⁾ (based on²⁵⁾), and also by SPF, the increasing importance of starbursts at high redshift, due to the increasing merger rate and higher gas fractions, is a natural mechanism to produce this population. The models of SPF contain a detailed treatment of mergers and the ensuing collisional starbursts, which

has been calibrated against the merger rate in cosmological N -body simulations ²⁶⁾ and the starburst efficiency in hydrodynamical simulations ^{27, 28)}. Moreover, they produced good agreement with observations of LBGs (e.g. ²⁹⁾) and damped Lyman- α systems (SPF and ³⁰⁾) as well as low redshift galaxies (SP). Therefore, it will be extremely interesting to see if these same models, when combined with the more sophisticated treatment of dust extinction and emission developed by Devriendt, Guiderdoni, and collaborators, will be able to simultaneously reproduce observations over the broad range of wavelengths and redshifts discussed above.

In the next section we briefly describe the ingredients of our models, and then present the results of the predicted EBL. Section 4 presents the implications for γ -ray attenuation, and §5 briefly discusses some alternative treatments and our own conclusions. The work summarized here is a brief, preliminary sample of the results which will soon be presented in a series of papers, now in preparation, on the EBL and its breakdown into various kinds of sources and on the implications for γ -ray astronomy.

2 Semi-analytic modelling

In this section we briefly describe the ingredients of our models. Readers can refer to SP and SPF for more details, and to ³³⁾ for a brief introduction.

Using the method described in ¹³⁾, we create Monte-Carlo realizations of the masses of progenitor halos and the redshifts at which they merge to form a larger halo. These “merger trees” reflect the collapse and merger of dark matter halos within a specific cosmology (each branching in the tree represents a halo merging event — for examples, see e.g. ³⁴⁾). We truncate the trees at halos with a minimum circular velocity of 40 km/s, below which we assume that the gas is prevented from collapsing and cooling by photoionization. Each halo at the top level of the hierarchy is assumed to be filled with hot gas, which cools radiatively and collapses to form a gaseous disk. The cooling rate is calculated from the density, metallicity, and temperature of the gas. Cold gas is turned into stars using several simple recipes, depending on the mass of cold gas present and the dynamical time of the disk. Supernovae inject energy into the cold gas and may expell it from the disk and/or halo if this energy is larger than the escape velocity of the system. Chemical evolution is traced assuming a constant yield of metals per unit mass of new stars formed. Metals

are initially deposited into the cold gas, and may later be redistributed by supernovae feedback, and mixed with the hot gas or the diffuse (extra-halo) inter-galactic medium.

When halos merge, the galaxies contained in each progenitor halo retain their separate identities either until they spiral to the center of the halo due to dynamical friction and merge with the central galaxy, or until they experience a binding merger with another satellite galaxy orbiting within the same halo. We take into account subhalo truncation due to tidal effects in the larger halo. All newly cooled gas is assumed to initially collapse to form a disk, and major (nearly equal mass) mergers result in the formation of a spheroid. New gas accretion and star formation may later form a new disk, resulting in a variety of bulge-to-disk ratios at late times.

For an assumed IMF, the stellar SED of each galaxy is then obtained using stellar population models. Here we use the multi-metallicity stellar SEDs of ¹²⁾ for the Salpeter and Kennicutt IMF cases, and the solar metallicity GISSEL models ³⁸⁾ for the Scalo IMF. (We have found that using evolving metallicity rather than solar metallicity SEDs has a relatively small impact on the resulting EBL.) Dust extinction is modelled using an approach similar to that of ¹¹⁾. The optical depth of the disk is assumed to be proportional to the column density of metals. We then use a simple slab geometry where stars and gas are homogeneously mixed, and assign a random inclination to each galaxy to compute the absorption. We use a metallicity dependent extinction curve, following ^{23, 11)}.

All absorbed light is re-radiated at longer wavelength. The galactic dust emission spectrum is represented by a combination of three components: 1) hot dust (as in H_{II} regions), 2) warm dust (as in the diffuse H_I), and 3) cold dust (as in molecular clouds). In the models of Devriendt et al. ¹²⁾, these components are modelled as a mixture of polycyclic aromatic hydrocarbon molecules (PAH), very small grains, and big grains. Big grains may be either cold (~ 17 K), or heated by radiation from star-forming regions (as suggested by observations of typical local starburst galaxies like M82). A set of template spectra is then constructed for galaxies of varying IR luminosity, with admixtures of the various components selected in order to reproduce the observed relations between IR/sub-mm color and IR luminosity. A similar approach was used by ³⁹⁾, using a mixture of a typical Orion-like H_{II} spectrum and an H_I spectrum

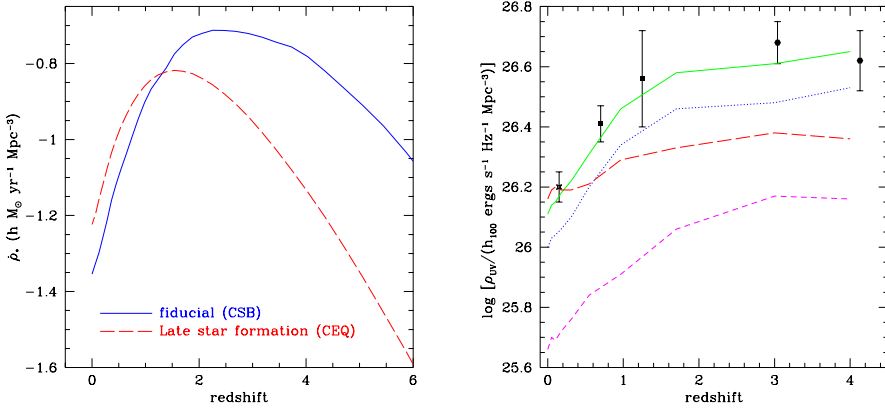


Figure 1: (a) The star formation rate density predicted by our models, for two different recipes of star formation. Both models produce about the same total mass density of stars by $z = 0$ (i.e., the areas under the curves are equal when they are plotted linearly vs. time), but the collisional starburst model (CSB) peaks at higher redshift. (b) Comoving luminosity density at 2000 \AA as a function of redshift. Data points represent the observed global luminosity density at rest $\sim 2000 \text{ \AA}$, obtained by integrating the observational best-fit Schechter luminosity functions over all luminosities ($\rho_L = \phi_* L_* \Gamma(2 - \alpha)$), including corrections for dust extinction. The $z = 0.15$ point is from ³¹, the $z \sim 0.4$ and 1.2 points are from ³², and the $z \sim 3$ and $z \sim 4$ points are from ¹⁷. The curves for our four models are labeled as in Figure 3. The model curves have been corrected for dust extinction using the approach described in the text.

constructed to fit DIRBE observations of the diffuse ISM ⁴⁰). Here, we use the more empirical emission templates of ³⁹) (kindly provided in electronic form by E. Dwek), but we obtain very similar results with the models of ¹²).

The recipes for star formation, feedback, chemical evolution, and dust optical depth contain free parameters, which we set for each model (see SP) by requiring an average fiducial “Milky Way” galaxy to have a K-band magnitude, cold gas mass, metallicity, and average B-band extinction as dictated by observations of nearby galaxies.

Figure 1a shows the global star formation rate density for the two star formation recipes that we consider here. The “fiducial” model is the collisional starburst (CSB) model favored by SPF, in which bursts of star formation may be triggered by galaxy collisions. The “Late Star Formation” model is the Constant Efficiency Quiescent (CEQ) model of SPF, in which cold gas is converted to stars only in a quiescent mode with constant efficiency. This produces a star formation history similar to the models of the Durham group ⁴¹), in which the

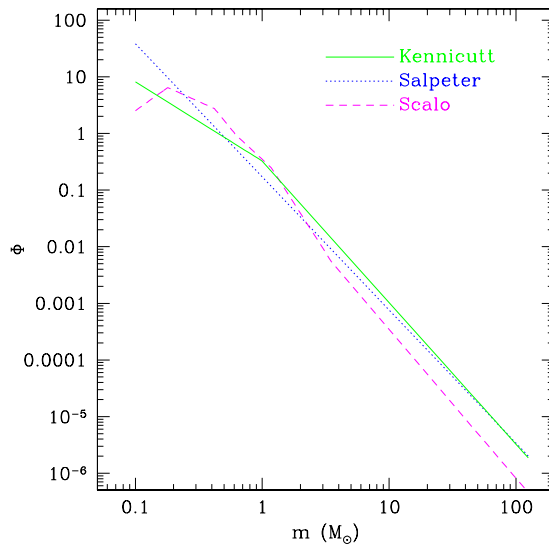


Figure 2: The three stellar Initial Mass Functions (IMFs) used here: Kennicutt ⁴⁴), Salpeter ⁴³), and Scalo ⁴²).

peak in the star formation history occurs at a more recent epoch ($z \sim 1.5$) than in the CSB model. For the CSB model, we consider three different choices of IMF: Scalo ⁴²⁾, Salpeter ⁴³⁾, and Kennicutt ⁴⁴⁾. These IMFs are graphed in Figure 2. For the CEQ model we show only the Kennicutt case. There is a noticeable difference in the far-UV and the mid- to far-IR. The Scalo IMF produces less UV light relative to optical and near-IR light, compared to the Kennicutt and Salpeter IMFs, which produce more high mass stars than the Scalo IMF, and thus more ultraviolet light to be absorbed and re-radiated by dust in the far IR. In Fig. 1b we show the redshift evolution of the far-UV (2000Å) luminosity density for these four models, compared with observations.² The Scalo model falls short at all redshifts, and the CEQ model, which agrees at $z = 0$, falls short at higher redshifts.³ It is encouraging that our very simple model for dust extinction, which we normalized in the B-band at $z = 0$, appears to yield the appropriate level of dust extinction in the UV at higher redshifts (SPF).

Recently, improved luminosity functions (LFs) have become available in optical bands from the Sloan Digital Sky Survey ⁴⁷⁾ and in the K-band from 2MASS ^{48, 49)}. We have found that our CSB model with Kennicutt IMF agrees well with all of these LFs when the average baryon fraction is $f_b = 0.1$. This model is also consistent with the number counts in the mid-IR (15 μm from ISOCAM ²¹⁾) and far IR (60 μm from IRAS, 175 μm from ISOPHOT) but not the sub-mm (850 μm from SCUBA ²²⁾). The resulting EBL is similar to that from the Salpeter model discussed below.

²These models were also compared with the observed luminosity density from nearby galaxies, obtained by integrating the luminosity functions of galaxies resolved in recent redshift surveys at wavelengths ranging from 0.2 to 2.2 μm , in Fig. 3 of ¹⁾. However, the SAM outputs graphed there were inadvertently multiplied by a factor of $h^4 \approx 0.25$. In ³³⁾, we renormalized all the models by requiring that they all agreed with the K-band point at 2.2 μm . Here we do not do this since our current SAMs ^{9, 10)} use a corrected version ⁴⁵⁾ of the Press-Schechter formalism.

³The Durham type models ⁴¹⁾ of SPF also predict that LBGs have higher stellar mass than observations indicate ²⁹⁾, while predicted stellar masses from the CSB model of SPF are in good agreement with the observations ⁴⁶⁾.

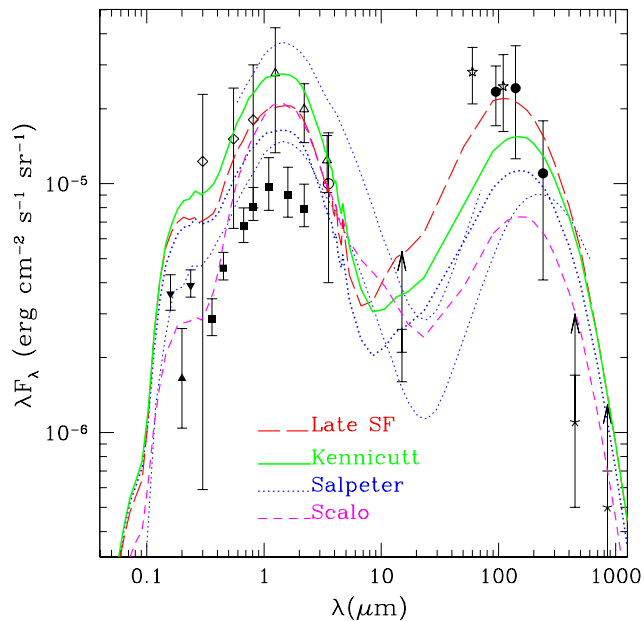


Figure 3: Extragalactic background light: models and data. The far-UV points are from STIS (inverted filled triangles) ⁵⁰⁾ and FOCA observations (filled triangle) ⁵¹⁾. The lower optical points (filled squares) are lower limits from resolved sources ²⁰⁾; the upper ones (open diamonds) are from absolute photometry ⁵²⁾. The near-IR points are from DIRBE: (open circle) ⁵³⁾, (open triangles) ⁵⁴⁾. The point at 15 μm is from ISOCAM resolved sources ²¹⁾, and is thus a lower limit. The far-IR points are from DIRBE (filled circles) ^{5, 55)}, (stars) ⁵⁶⁾. The curves are our results from modelling the history of star formation in the ΛCDM cosmology using semi-analytic methods: a model with both quiescent star formation with constant efficiency and starbursts, with Kennicutt, Salpeter, and Scalo IMFs, and a Late SF model with only quiescent star formation with constant efficiency (CEQ). The lower light dotted curve is the ΛCDM EBL calculated using our previous methods ³³⁾ for the Salpeter IMF, and the upper one is the same curve to 80 μm multiplied by 2.5 for comparison with Mrk 501 data as analyzed by ⁶²⁾ (see text). Note that $10^{-6} \text{ erg s}^{-1} \text{ cm}^{-2} \text{ sr}^{-1} = 1 \text{ nW m}^{-2} \text{ sr}^{-1}$.

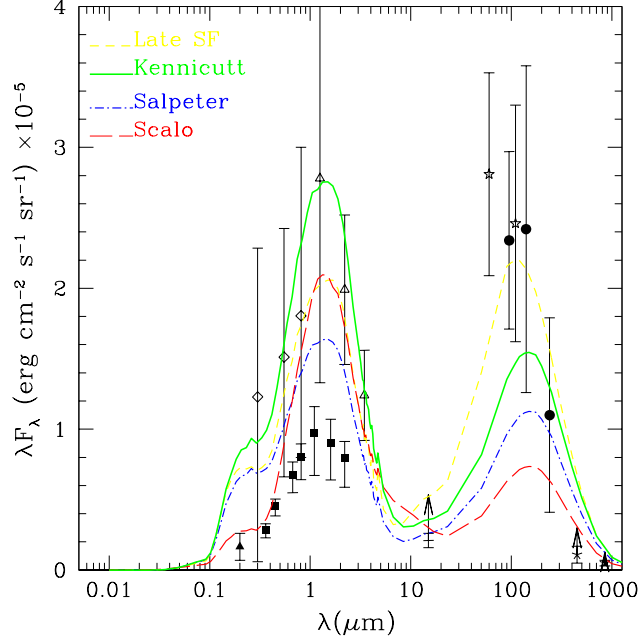


Figure 4: Extragalactic background light: models and data with linear vertical axis. Labels are as in Fig. 3.

3 The Integrated Extragalactic Background Light

Figure 3 shows the EBL produced by our four models, obtained by integrating the light over redshift (out to $z = 4$) with the appropriate K-corrections due to cosmological redshifting. We compare this with a compilation of observational limits and measurements of the EBL. Fig. 4 presents the same four models and the same data, but with a linear rather than logarithmic vertical axis so that one can integrate the total energy in the EBL by eye. It is apparent that there is at least as much energy in the far-IR part of the EBL as in the entire optical and near-IR bands. For example, Puget and collaborators ²⁾ estimated that the total energy in the EBL is between 60 and $93 \text{ nW m}^{-2} \text{ sr}^{-1}$, with between 20 and $41 \text{ nW m}^{-2} \text{ sr}^{-1}$ contributed by the optical and near-IR, and between 40 and $52 \text{ nW m}^{-2} \text{ sr}^{-1}$ coming from the far-IR. If the possible detection of

the EBL at $60 \mu\text{m}$ by Finkbeiner et al. ⁵⁶⁾ were correct, that would further increase the far-IR EBL; however, it is very difficult to determine the EBL at $60 \mu\text{m}$ since the zodiacal light is so much brighter at that wavelength, and it was probably partly confused with the EBL ⁵⁷⁾.

The total energy in the EBL in units of critical density ρ_c is $\Omega_{\text{EBL}} = (4\pi/c)(I_{\text{EBL}}/\rho_c c^2) = 2.5 \times 10^{-8} I_{\text{EBL}} h^{-2}$, where I_{EBL} is in units of $\text{nW m}^{-2} \text{sr}^{-1}$. The total energy density in the EBL corresponding to the lower and upper estimates of ²⁾ is $\Omega_{\text{EBL}} = (3.6 - 5.5) \times 10^{-6} (h/0.65)^{-2}$. Although the EBL includes energy radiated by active galactic nuclei (AGNs) as well as stars, it is unlikely that AGNs contributed more than a few percent of the total. This is because the total energy radiated by AGNs is $E_{\text{EBL}}^{\text{AGN}} = \eta \rho_{\text{BH}} c^2$, where the efficiency of conversion of mass to radiated energy in AGNs is $\eta \sim 0.05$. Correspondingly, $\Omega_{\text{EBL}}^{\text{AGN}} = \eta \Omega_{\text{BH}} (1 + z_{\text{BH}})^{-1} \approx 4.5 \times 10^{-8} h^{-1} (\eta/0.05) [3/(1 + z_{\text{BH}})] \lesssim 0.02 \Omega_{\text{EBL}}$. ⁴ So for simplicity, in this paper we will neglect the contribution of AGNs to the EBL.

Several interesting features emerge from the comparison of our SAM models with the EBL data. In the UV to near-IR, the models are closer to the direct measures of the EBL obtained by ^{52, 53, 54)} than to the lower limits from the Hubble Deep Field ²⁰⁾, although the Salpeter IMF produces less light in the UV because it has fewer high-mass stars. As noted, our Kennicutt CSB SAM with $f_b = 0.1$, which agrees well with the latest observed local luminosity density at $z = 0$, produces an EBL close to the Salpeter one in Fig. 4. Of our four new EBL curves, the Late SF model and the fiducial Kennicutt model are also consistent with the DIRBE measurements at $140 \mu\text{m}$. The Salpeter EBL lies a little more than 2σ below the DIRBE measurement at $140 \mu\text{m}$. The LateSF far IR is higher than the other models because its later star formation suffers less dilution due to the expansion of the universe. The models differ significantly in the mid-IR, $\sim 10 - 60 \mu\text{m}$, where the EBL can be probed by TeV γ -rays. The lower dotted curve in Fig. 3, representing our previous attempt ³³⁾ to

⁴Updating ⁵⁸⁾, we have estimated $\Omega_{\text{BH}} = (M_{\text{BH}}/M_{\text{spheroid}})\Omega_{\text{spheroid}} \approx (1.5 \times 10^{-3})(1.8 \times 10^{-3} h^{-1})$, using the observed (loose) correlation ⁵⁹⁾ between a black hole mass and that of the galactic spheroid in which it is found, and the estimated cosmological density of spheroids ⁶⁰⁾. Note that the factor $(1+z)^{-1}$ arises because of the dilution of the contribution of high-redshift sources due to the expansion of the universe.

model the EBL, is well below the $15 \mu\text{m}$ lower limit as well as the DIRBE measurements at longer wavelengths. As we stated in [33](#)), we expected our EBL results to change as we improved our dust emission modelling. In addition to inclusion of the PAH features, the new dust emission model has more warm dust than the one used in [33](#)).

We now discuss constraints from the TeV γ -ray observations.

4 Attenuation of high-energy γ -rays

Figure 5 shows the γ -ray attenuation predicted by the four ΛCDM models considered here, for sources at redshifts $z_s = 0.03$ and 0.10 . All of the models predict rather little absorption at $E_\gamma \lesssim 5 \text{ TeV}$ for sources at $z_s = 0.03$, but

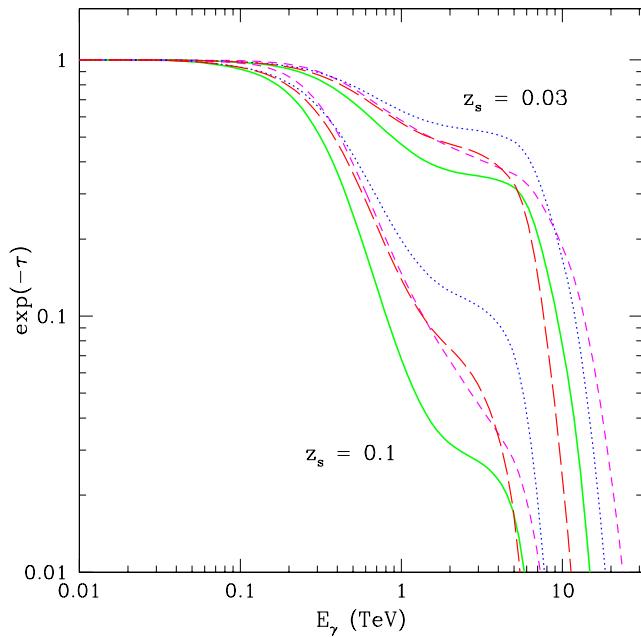


Figure 5: The attenuation factor, $\exp(-\tau)$ for γ -rays as a function of γ -ray energy for the four ΛCDM models considered in Fig. 4. The assumed redshift of the source, z_s , is indicated for each set of curves.

fairly sharp cutoffs above ~ 5 TeV, especially for the Late SF model. That model may be in conflict with the data from Mrk 501. For the blazars Mrk 421 and 501, both at $z \approx 0.03$, the synchrotron self-Compton (SSC) model, in which \sim keV synchrotron X-radiation from a very energetic electron beam is Compton up-scattered by the same electrons to produce the observed \sim TeV γ -rays, appears to explain both the keV-TeV spectra and their time variation (see, e.g., ^{62, 63}) and references therein). Using a simplified SSC model and keV X-ray data to predict the unattenuated TeV spectrum of Mrk 501, Guy et al. ⁶²) used CAT and HEGRA data to estimate the amount of γ -ray attenuation. They find that there is a rather good fit to the observed attenuation for the Λ CDM-Salpeter EBL from our earlier work ³³) when it is scaled upward by a factor of up to about 2.5 across the wavelength range 1-80 μ m; this is the upper Salpeter curve on Fig. 3. Our new Salpeter curve appears to be rather consistent with this rescaling of our old Salpeter one, the Kennicutt curve may be a little high, and the Late SF curve appears to be definitely too high. As noted earlier, the new Salpeter EBL curve in Figs. 3,4 is similar to our latest $f_b = 0.1$ Kennicutt SAM, which is in good agreement with the latest local luminosity functions in the optical and K bands from SDSS and 2MASS, and also in good agreement with IR number counts from IRAS and ISO satellites.

The large flares in Mrk 501 in spring 1999 allowed an accurate measurement of the gamma ray spectrum up to about 17 TeV, and indicated that the spectrum had an exponential cutoff at about 5 TeV ⁶⁴). The flaring activity in Mrk 421 in early 2001 has now provided evidence for an exponential cutoff at about 4 TeV ⁶⁵). The coincidence in the cutoffs (within observational uncertainties) for these two different extragalactic sources suggests that both are due to absorption via pair production on the EBL. In order to confirm this, it will of course be necessary to see similar cutoffs at lower energies for blazars at greater distances. There are already indications of this from 1426+42, a blazar at redshift $z = 0.13$ (four times farther than Mrk 421), on which there is enough data from CAT ⁶⁶), Whipple ⁶⁷), and HEGRA ⁶⁸) to begin to determine the spectrum from a few hundred GeV to several TeV. It will be very useful to measure the spectrum from this and other sources at comparable distances, such as PKS2155-304 at $z = 0.116$, which will soon be possible with the next generation of atmospheric Cherenkov telescopes such as the H.E.S.S. array in Namibia, the CANGAROO-III array in Australia, and the VERITAS array in

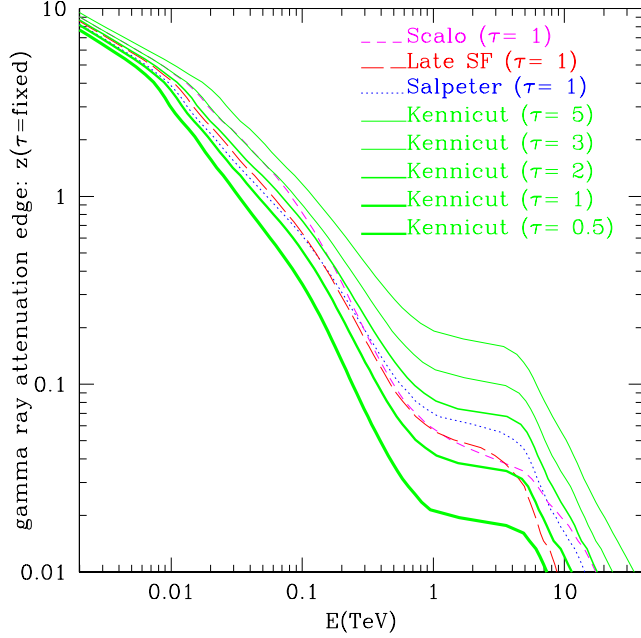


Figure 6: The γ -ray attenuation edge. The redshift where the optical depth reaches unity is shown as a function of γ -ray energy for each of the four Λ CDM models considered in Fig. 4. Also shown for the Kennicutt IMF is the redshift where the optical depth equals 0.5, 2, 3, and 5.

Arizona.

Assuming that the EBL is like the LateSF curve in Figs. 3,4, several authors (e.g. ⁶⁹) have argued that the TeV attenuation that this implies plus the observed spectrum of Mrk 501 leads to the requirement that the spectrum at the source have a strong upturn in its emitted flux above about 15 TeV, which would be very hard (although perhaps not impossible ⁷¹) to understand, and they even suggest that one might have to abandon Lorentz invariance. However, if one instead assumes our Salpeter EBL in Fig. 4 and applies an SSC analysis to the HEGRA data from the Mrk 501 flares in 1997, the implied source spectrum is very reasonable, without an upturn at the high-energy end ⁷²).

The compatibility of our new EBL calculations with the available data

on TeV γ -ray attenuation is definitely worth further investigation. The results appear to be sensitive to the details of the models, raising the hope that they may be able to help answer important questions about star formation and dust reradiation, and also help to test the SSC modelling.

Figure 6 depicts the γ -ray “absorption edge,” the redshift of a source corresponding to an optical depth of unity, as a function of γ -ray energy. Travelling through the evolving extragalactic radiation field, γ -rays from sources at lower redshift suffer little attenuation. The universe becomes increasingly transparent as E_γ decreases, probing the background light at increasingly short wavelengths. (We are using the treatment of ⁶¹) to account for absorption of ionizing radiation by the Lyman alpha forest.) The models all have the same qualitative features, but differ significantly quantitatively. The location of the absorption edge is affected both by the assumed IMF and by the history of star formation. There is more absorption at most redshifts with the Kennicutt IMF because with a higher fraction of high mass stars, it is more efficient at producing radiation for a given stellar mass; there is more absorption nearby in the Late SF model because the starlight in this model is less diluted by the expansion of the universe. It is possible that measuring the transparency of the universe to γ -rays at ~ 100 GeV with a number of sources at various redshifts can provide a strong probe of star formation, although there are uncertainties due to extinction by dust.

5 Outlook

The semi-analytic modelling of the EBL described here follows the evolution of galaxy formation in time. Forward modelling is a more physical approach than backward modelling (luminosity evolution). Pure luminosity evolution (e.g., ^{73, 74, 70}) assumes that the entire evolution of the luminosity of the universe arises from galaxies in the local universe just becoming brighter at higher redshift by some power of $(1+z)$ out to some maximum redshift. It effectively assumes that galaxies form at some high redshift and subsequently just evolve in luminosity in a simple way. This is at variance with hierarchical structure formation of the sort predicted by CDM-type models, which appears to be in better agreement with many sorts of observations.

An alternative approach to modelling the EBL has been followed by Pei and collaborators ^{75, 76, 77}, in which they find an overall fit to the global

history of star formation subject to constraints from input data including the evolution of the amount of neutral hydrogen in damped Ly α systems (DLAS). Their first attempt (75, 76), which was used as the basis for EBL estimates by (39, 78), was somewhat misled by the sharp drop in the DLAS hydrogen abundance from redshift $z \sim 3$ to $z \sim 2$ reported in (79). With more complete data on DLAS (see, e.g., Fig. 14 of (80)) the $z = 3$ point is lower and the neutral hydrogen abundance is almost constant from $z = 2$ to 4. The latest paper by Pei et al. (77) takes a variety of recent data into account. Their approach is to follow the evolution of the total mass in stars, interstellar gas, and metals in a representative volume of the universe; they assume a Salpeter IMF. By contrast, the semi-analytic methods we use follow the evolution of many individual galaxies in the hierarchically merging halos of specific CDM models, here Λ CDM. Despite the differences in approach, and the fact that (77) assumed $\Omega_m = 1$ and Hubble parameter $h = 0.5$, their results are broadly similar to those from the semi-analytic approach (see their §4.4). In particular, their EBL is similar to our old results (33) for the Salpeter IMF. Our EBL results presented here are higher in the near-IR and more consistent with the direct determinations (53, 54); they are also higher in the mid-IR, probably mainly because of the warm dust and PAH features in our dust emission model. It will be interesting to see whether further development of the global approach of Pei et al. and of the semi-analytic approach lead to convergent results.

As our calculations show, the EBL, especially at $\lesssim 1 \mu\text{m}$ and $\gtrsim 10 \mu\text{m}$, is significantly affected by the IMF and the absorption of starlight and its reradiation by dust, as well as by the underlying cosmology. The cosmological parameters are becoming increasingly well determined by other observations. As data become available on γ -ray emission and absorption from sources at various redshifts, especially from the new generation of Atmospheric Cherenkov Telescopes and the new γ -ray satellites AGILE and GLAST, these data and their theoretical interpretation will help to answer fundamental questions concerning how and in what environments all the stars in the universe formed.

Acknowledgments

I thank my collaborators Rachel S. Somerville, James S. Bullock, and Julien E. G. Devriendt. My work was supported by NASA and NSF grants at UCSC. I am grateful for a Humboldt Award, and I thank Leo Stodolsky for hospitality

and Eckart Lorenz for enlightening discussions about γ -ray astronomy at the Max-Planck-Institut für Physik, München. I also thank Simon White for hospitality at MPI Astrophysics in Garching, and Heinz Völk for hospitality at MPI Nuclear Physics in Heidelberg. I thank Henric Krawczynski, Paolo Coppi, and Felix Aharonian for very helpful discussions of their SSC modelling. I thank Aldo Morselli for inviting me to give these lectures at the ISSS, and for his patience in waiting for me to send him the written versions.

References

1. J.R. Primack, R.S. Somerville, J.S. Bullock, and J.E.G. Devriendt, in *High Energy Gamma Ray Astronomy*, Proceedings of the International Symposium Gamma-2000, Heidelberg, June 2000, eds. F. Aharonian and H. Völk, AIP Conf. Proc., Vol. 558, pp. 463-478 (2001).
2. R. Gispert, G. Lagache, and J.L. Puget, *A&A* **360**, 1 (2000).
3. J.L. Puget et al., *A&A* **308**, L5 (1996).
4. B. Guiderdoni et al., *Nature* **390**, 257 (1997).
5. M.G. Hauser et al., *ApJ* **508**, 25 (1998).
6. D.J. Fixsen et al., *ApJ* **508**, 123 (1998).
7. G. Kauffmann, S.D.M. White, and B. Guiderdoni, *ApJ* **264**, 201 (1993).
8. S. Cole et al., *MNRAS* **271**, 781 (1994).
9. R.S. Somerville and J.R. Primack, *MNRAS* **310**, 1087 (1999). (SP)
10. R.S. Somerville, J.R. Primack, and S.M. Faber, *MNRAS* **320**, 504 (2001). (SPF)
11. J.E.G. Devriendt and B. Guiderdoni, *A&A* **363**, 851 (2000).
12. J.E.G. Devriendt, B. Guiderdoni, and R. Sadat, *A&A* **350**, 381 (1999).
13. R.S. Somerville and T. Kolatt, *MNRAS* **305**, 1 (1999).
14. R.S. Somerville, G. Lemson, T. Kolatt, and A. Dekel, *MNRAS* **316**, 479 (2000).

15. J.R. Primack, "Cosmological Parameters 2000," in *Sources and Detection of Dark Matter in the Universe*, Proc. 4th International Symposium (DM 2000), Marina del Rey, California, 20-23 Feb 2000, ed. D. Cline (Berlin: Springer, 2001), pp. 3-17 — and also my other lectures in these ISSS proceedings.
16. F.R. Pearce et al., *MNRAS* **326**, 649 (2000).
17. C. Steidel et al., *ApJ* 519, 1 (1999).
18. D.B. Sanders, *Astrophys. and Space Sci.* **269/270**, 381 (1999).
19. B.G. Soifer and G. Neugebauer, *AJ* **101**, 354 (1991).
20. P. Madau and L. Pozzetti, *MNRAS* **312**, L9 (2000).
21. D. Elbaz et al., *A&A Letters* **351**, L37 (1999).
22. A. Blain, I. Smail, R.J. Ivison, and J.-P. Kneib, *MNRAS* 302, 632 (1999).
23. B. Guiderdoni, E. Hivon, F.R. Bouchet, and B. Maffei, *MNRAS*, **295**, 877 (1998).
24. J. Silk and J. Devriendt, (2000) in in Proc. IAU Symp. 204 *The Extragalactic Infrared Background and its Cosmological Implications*, eds M. Harwit and M.G. Hauser (Astronomical Society of the Pacific, San Francisco, 2001).
25. C. Balland, J. Silk, and R. Schaeffer *ApJ* **497**, 541 (1998).
26. T. Kolatt et al., astro-ph/0010222 (2000).
27. C. Mihos and L. Hernquist, L. *ApJ* **425**, 13 (1994); **448**, 41 (1995); **464**, 641 (1996).
28. R.S. Somerville et al., in XVth IAP Meeting, Dynamics of Galaxies ed. F. Combes et al., ASP Conf. Series **197**, 331 (1999).
29. C. Papovich, M. Dickinson, and H.C. Ferguson, *ApJ*, **559**, 620 (2001).
30. A.H. Maller, J.X. Prochaska, R.S. Somerville, and J.R. Primack, *MNRAS* **326**, 1475 (2001).

31. M. Sullivan et al., *MNRAS* **312**, 442 (2000).
32. L.L. Cowie, A. Songaila, and A.J. Barger, *AJ* **118**, 603 (1999).
33. J.R. Primack, J.S. Bullock, R.S. Somerville, and D. MacMinn, *Astroparticle Phys.* **11**, 93 (1999); J.S. Bullock, R.S. Somerville, D. MacMinn, and J.R. Primack, *Astroparticle Phys.* **11**, 111 (1999).
34. R.H. Wechsler, J.S. Bullock, J.R. Primack, A.V. Kravtsov, and A. Dekel, *ApJ* in press, astro-ph/0108151 (2001).
35. S.R. Folkes et al., *MNRAS* **308**, 459 (1999).
36. M.J. Geller et al., *AJ* **114**, 2205 (1997).
37. J.P. Gardner, R.M. Sharples, C.S. Frenk, and B.E. Carrasco, *ApJ* **480**, L99 (1997).
38. G. Bruzual and S. Charlot, *ApJ*, **405**, 538 (1993).
39. E. Dwek et al., *ApJ* **508**, 106 (1998).
40. E. Dwek et al., *ApJ* **484**, 779 (1997).
41. C.M. Baugh, S. Cole, C.S. Frenk, and C.G. Lacey, *ApJ* **498**, 504 (1998).
42. J.M. Scalzo *Fund. Cosmic Phys.* **11**, 1 (1986).
43. E.E. Salpeter, *ApJ* **121**, 161 (1955).
44. R.E. Kennicutt, *ApJ* **272**, 54 (1983).
45. R. Sheth, and G. Tormen, *MNRAS* **308**, 119 (1999).
46. J.R. Primack, in *Proc. Galaxy Masses at Low and High Redshift* (Venice October 2001), eds. R. Bender and A. Renzini (Springer-Verlag, 2002), in prep.
47. M.R. Blanton et al., *AJ* **121**, 235 (2001).
48. C.S. Kochanek et al., *ApJ* **560**, 566 (2001).
49. S. Cole et al., *MNRAS* **326**, 255 (2001).

50. J.P. Gardner, T.B. Brown, and H.C. Ferguson, *ApJ* **542**, L79 (2000).
51. C. Armand, B. Milliard, and J.-M. Deharveng, *A&A* **284**, 12 (1994).
52. R.A. Bernstein, W.L. Freedman, and B.F. Madore, *ApJ* submitted (2001).
53. E. Dwek and R.G. Arendt, *ApJ* **508**, L9 (1998).
54. V. Gorjian, E.L. Wright, and R.R. Chary, *ApJ* **536**, 550 (2000); E.L. Wright, astro-ph/0004192 (2000).
55. G. Lagache et al. in *ISO Surveys of a Dusty Universe*, ed. D. Lemke et al., Springer Lecture Notes in Physics **548**, 81 (2000).
56. D.P. Finkbeiner, M. Davis, and D. Schlegel, *ApJ* **544**, 81 (2000).
57. D.P. Finkbeiner, in Proc. IAU Symp. 204 *The Extragalactic Background and its Cosmological Implications*, eds. M. Harwit and M.G. Hauser (Astronomical Society of the Pacific, San Francisco, 2001), p. 121.
58. P. Madau, *VLT Opening Symposium* ed. J. Bergeron et al. (Springer, Berlin, 2000), p. 52.
59. J. Kormendy, astro-ph/0007401 (2000).
60. M. Fukugita, C. Hogan, and P.J.E. Peebles, *ApJ* 503, 518 (1998).
61. P. Madau, *ApJ*, 441, 18 (1995).
62. J. Guy, C. Renault, F.A. Aharonian, M. Rivoal, and J.-P. Tavernet, *A&A* **359**, 419 (2000).
63. H. Krawczynski, P.S. Coppi, T. Maccarone, and F.A. Aharonian, *A&A* **353**, 97 (1999).
64. F. Aharonian et al., *ApJ* **546**, 898 (2001).
65. F. Krennrich et al., *ApJ* **560**, 45 (2001).
66. A. Djannati-Atai et al., in *Proc. ICRC-2001*.
67. D. Horan et al., submitted to *ApJ* (2001).
68. F. Aharonian, in *Proc. ICRC-2001*, astro-ph/0112314 (2001).

69. R.J. Protheroe and H. Meyer, *Phys. Lett.* **B493**, 1 (2000).
70. F. Stecker, in Proc. IAU Symp. 204 *The Extragalactic Background and its Cosmological Implications*, eds. M. Harwit and M.G. Hauser (Astronomical Society of the Pacific, San Francisco, 2001).
71. F. Aharonian, A.N. Timokhin, and A.V. Plyasheshnikov, *A&A* in press, astro-ph/0108419 (2001).
72. H. Krawczynski, P. Coppi, and F. Aharonian, submitted (2001).
73. M.A. Malkan and F.W. Stecker, *ApJ* 496, 13 (1998).
74. M.A. Malkan and F.W. Stecker, *ApJ* **555**, 641 (2001).
75. Y.C. Pei and S.M. Fall, *ApJ* **454**, 69 (1995).
76. S.M. Fall, S. Charlot, and Y.C. Pei, *ApJ* **464**, L43 (1996).
77. Y.C. Pei, S.M. Fall, and M.B. Hauser, *ApJ* **522**, 604 (1999).
78. M.W. Salamon and F.W. Stecker, *ApJ* **493**, 547 (1998).
79. K.M. Lanzetta, A.M. Wolfe, and D.A. Turnshek, *ApJ* **440**, 435 (1995).
80. L. Storrie-Lombardi and A.M. Wolfe, *ApJ* **545**, 603 (2000).